



RESEARCH

Open Access



# Reawakening inflammation in the chronically injured spinal cord using lipopolysaccharide induces diverse microglial states

Rebecca K. John<sup>1</sup>, Sadie P. Vogel<sup>1</sup>, Sameera Zia<sup>1</sup>, Kelly V. Lee<sup>3</sup>, Antoinette T. Nguyen<sup>2</sup>, Abel Torres-Espin<sup>2,6</sup>, Keith K. Fenrich<sup>1,2</sup>, Carmen Ng<sup>1</sup>, Emma K. A. Schmidt<sup>1</sup>, Romana Vavrek<sup>2</sup>, Pamela J. F. Raposo<sup>2</sup>, Keira Smith<sup>1</sup>, Karim Fouad<sup>1,2\*</sup>  and Jason R. Plemel<sup>1,3,4,5\*</sup> 

## Abstract

**Background** Rehabilitative training is an effective method to promote recovery following spinal cord injury (SCI), with lower training efficacy observed in the chronic stage. The increased training efficacy during the subacute period is associated with a shift towards a more adaptive or reparative state induced by the SCI. A potential link is SCI-induced inflammation, which is elevated in the subacute period, and, as injection of lipopolysaccharide (LPS) alongside training improves recovery in chronic SCI, suggesting LPS could reopen a window of plasticity late after injury. Microglia may play a role in LPS-mediated plasticity as they react to LPS and are implicated in facilitating recovery following SCI. However, it is unknown how microglia change in response to LPS following SCI to promote neuroplasticity.

**Main body** Here we used single-cell RNA sequencing to examine microglial responses in subacute and chronic SCI with and without an LPS injection. We show that subacute SCI is characterized by a disease-associated microglial (DAM) signature, while chronic SCI is highly heterogeneous, with both injury-induced and homeostatic states. DAM states exhibit predicted metabolic pathway activity and neuronal interactions that are associated with potential mediators of plasticity. With LPS injection, microglia shifted away from the homeostatic signature to a primed, translation-associated state and increased DAM in degenerated tracts caudal to the injury.

**Conclusion** Microglial states following an inflammatory stimulus in chronic injury incompletely recapitulate the subacute injury environment, showing both overlapping and distinct microglial signatures across time and with LPS injection. Our results contribute to an understanding of how microglia and LPS-induced neuroinflammation contribute to plasticity following SCI.

**Keywords** Microglia, Spinal cord injury, Inflammation, Single-cell RNA sequencing, Plasticity, Lipopolysaccharide, Chronic nervous system injury

\*Correspondence:

Karim Fouad

kfouad@ualberta.ca

Jason R. Plemel

jrplemel@ualberta.ca

Full list of author information is available at the end of the article



© The Author(s) 2025. **Open Access** This article is licensed under a Creative Commons Attribution-NonCommercial-NoDerivatives 4.0 International License, which permits any non-commercial use, sharing, distribution and reproduction in any medium or format, as long as you give appropriate credit to the original author(s) and the source, provide a link to the Creative Commons licence, and indicate if you modified the licensed material. You do not have permission under this licence to share adapted material derived from this article or parts of it. The images or other third party material in this article are included in the article's Creative Commons licence, unless indicated otherwise in a credit line to the material. If material is not included in the article's Creative Commons licence and your intended use is not permitted by statutory regulation or exceeds the permitted use, you will need to obtain permission directly from the copyright holder. To view a copy of this licence, visit <http://creativecommons.org/licenses/by-nc-nd/4.0/>.

## Background

Traumatic spinal cord injury (SCI) is a devastating event that results in motor, autonomic and sensory deficits below the level of injury. One of the most effective methods of eliciting motor recovery after SCI is through rehabilitative training [1, 2]. Rehabilitative motor training boosts neural plasticity, enabling spared spinal cord circuitry to reconnect and restore lost functions [3]. Training has been shown to be more effective in the early stages after SCI, with lower training efficacy in chronic stages after injury [4–6], which is problematic after traumatic SCI because other concomitant trauma and focus on establishing essential skills may prevent people from early motor training. Differences in training efficacy are associated with changes in plasticity-promoting factors following SCI; for example, Chen and colleagues found neurotrophin-3 overexpression was associated with axonal sprouting in the subacute, but not chronic SCI environment [7]. However, the efficacy of rehabilitative training after SCI can be modified in task-specific [8, 9] and intensity-specific manner [10, 11]; all of which interact in a dynamic injury microenvironment [12].

Following SCI, the lesion environment changes with time, with ongoing secondary damage in the acute phase [13, 14], a subacute period characterized by a complex interaction of immune and glial cells that surround peripheral immune cells and form a glial and fibrotic scar [15]. This is followed by a chronic phase defined by stabilization of inflammatory processes [16] and a plateau in recovery [17]. These phases after injury also correspond to changes in training efficacy, with training efficacy highest in the subacute period and declining into the chronic period [4], suggesting that training efficacy and inflammatory responses may be linked.

An inflammatory stimulus re-establishes axonal sprouting in the chronic injury environment [18], further supporting the neuroimmune axis participating in training efficacy. Both Torres-Espín and colleagues and Zhong and colleagues found that an injection of lipopolysaccharide (LPS) with a chronic SCI enabled increased sprouting, alongside improvements in training efficacy in the chronic stage, suggesting that inducing an inflammatory stimulus could re-open the ‘window of opportunity’ for efficient training and allow for improved functional recovery [11, 19]. Therefore, changes in inflammation that occur across the time course of SCI likely play a role in regulating plasticity and functional recovery. Consistent with a role in promoting plasticity, augmenting inflammation promotes axonal growth following optic nerve injury. Eliciting an immune cell response via either a lens injury or the injection of zymosan increases retinal ganglion cell regeneration after optic nerve axotomy [20–22]. Retinal ganglion cell regeneration is stimulated by

macrophage- and neutrophil-derived growth factors [23], including oncomodulin [24–26], ciliary neurotrophic factor, interleukin-6, or leukemia inhibitory factor [27–29], suggesting that immune cells can act directly on neurons to promote plasticity or regeneration.

The immune system plays a dynamic and complex role following SCI, with dichotomous roles in exacerbating tissue damage and lesion pathology [30–32]; alongside enabling regeneration [33, 34]. Among the first cells to respond to injury, microglia (the innate immune cell of the central nervous system) play vital roles in orchestrating cellular inflammatory responses [35], as well as in forming the fibrotic glial scar [36] and clearing cellular debris [38]. Microglial depletion has been linked to poorer functional recovery after SCI [35, 36, 39, 40]. In addition to roles in facilitating recovery, microglia also react to LPS injection in SCI [11], which makes them a promising candidate to contribute to LPS-mediated plasticity.

In recent years, it is becoming increasingly understood that microglia take on several distinct states that change throughout disease processes [41]. Using single-cell RNA sequencing (scRNAseq) it is possible to examine this complex microglial response in a variety of disease and injury conditions, revealing a highly diverse set of microglial signatures [42–49], including in SCI [35, 40, 50–53].

Here we use scRNAseq to understand the microglial states during periods of high training efficacy (subacute SCI) and low training efficacy (chronic SCI), as well as how the microglial response changes with training efficacy and plasticity-promoting LPS treatment. Overall, we find microglial responses undergo transcriptional shifts from the subacute to the chronic time periods after SCI. The subacute period was hallmarked by a shift away from homeostatic signatures towards injury-induced states, including proliferative and disease-associated microglia. Several injury-induced states were retained into the chronic period after injury, although at lower levels than subacute injury, and this was accompanied by a shift back towards homeostatic microglial states. Inducing an inflammatory stimulus can enable improved training efficacy in the chronic period and was associated with a shift away from homeostatic microglial states towards a primed, translation-associated phenotype.

## Main text

### Materials and methods

#### Animals

Adult female Lewis rats (Charles River) were group housed and fed food and water ad libitum. 20 animals were utilized for single-cell RNA sequencing experiments (n=5/group). An additional 24 animals were utilized for immunofluorescence staining of the spinal cord (n=6/

group). All animal studies were conducted in accordance with the Canadian Council on Animal Care Guidelines and Policies with approval from the Animal Care and Use Committee: Health Sciences for the University of Alberta under AUP #254.

### **Spinal cord injury**

Animals received a dorsolateral quadrant injury at the cervical spinal cord (C4). Rats were anesthetized using isoflurane (5% isoflurane in 50:50 air:oxygen mixture for induction and 2.5% for maintenance). The dorsal neck was shaved, and the skin and muscle incised. A laminectomy at C4 was performed and a cervical dorsolateral transection injury was performed with a custom blade. Muscle and skin were closed using sutures and staples, respectively. Following surgery, 3 mL of saline was injected subcutaneously to rehydrate the animal and buprenorphine (0.03 mg/kg) was injected to manage post-operative pain for 1–2 days.

### **LPS injection**

LPS was derived from *Escherichia coli* endotoxin (serotype 055:B5, Sigma-Aldrich, L2880-10 MG) and dissolved in sterile saline (pyrogen-free 0.9% saline, Hospira). Rats were injected intraperitoneally with 0.5 mg/kg LPS or an injection of sterile saline 3 days prior to perfusions. Following injection, animals were monitored for sickness behaviour for 3 days.

### **Perfusions**

For immunofluorescence staining of the spinal cords, rats ( $n=24$ ) were euthanized with pentobarbital (Euthanyl, Bimeda-MTC, Animal-Health Inc.), and transcardially perfused with saline containing 0.02 g heparin/L (Millipore-Sigma, H4784), followed by fixation with 4% formalin (Sigma, 441,244–1 kg) in 0.1 M phosphate buffer. Spinal cords were dissected, and post-fixed overnight in a 4% formalin solution with 5% sucrose (Fischer Scientific, S5-3) and then placed in a 30% sucrose solution for 3 days. Tissue was then cut into a 2 cm section surrounding the injury site and frozen in 2-methylbutane (Fischer Scientific, O3551-4) at  $-60^{\circ}\text{C}$ .

### **Immunofluorescence**

Tissue was sectioned sagittally in 2 cm sections around the lesion site at  $25\ \mu\text{m}$  on a cryostat (Leica CM30505) onto ColorFrostPlus (Fisherbrand, Fisher Scientific) slides and stored at  $-20^{\circ}\text{C}$ . Tissue was warmed for 30 min on a slide warmer at  $37^{\circ}\text{C}$ . Subsequently, tissue was washed for 10 min in 0.01 M phosphate buffer saline (PBS; Sigma, P0017-100TAB), and then twice for 10 min with PBS with 0.03% Triton X-100 (PBST; Fisher Scientific, BP151-100). Slides were blocked with 10% Normal

Donkey Serum (Sigma-Aldrich, D9663) and PBST for 60 min at room temperature. Following this, slides were incubated with the primary antibodies (Goat anti-Iba1 [1:300, Novus Biologicals, NB100-1028], Mouse anti-Galectin3 [Gal3; 1:200; Invitrogen, MA1-940], Mouse anti-Cd74 [1:50, Santa Cruz Biotechnology, sc-53062] or Rabbit anti-Iba1 [1:1000, Wako, 019-19741]) overnight at room temperature. Iba1 was used to mark microglia/macrophages, while Gal3 and Cd74 were both identified in our scRNAseq results to demarcate populations of microglia. After the incubation with the primary antibody, tissue was again washed three times for 10 min with PBST. Slides were incubated with the secondary antibody (donkey anti-goat 488 [1:500; Jackson ImmunoResearch, 705-546-147], donkey anti-mouse 647 [1:500; Jackson ImmunoResearch, 715-606-151], donkey anti-rabbit 488 [1:500, Jackson ImmunoResearch, 711-546-152] for 2 h at room temperature. Slides were then washed twice with PBST and twice with PBS, each for 10 min; subsequently, slides were coverslipped (Fisherbrand, 1,255,020) and mounted with fluoromount containing DAPI (Invitrogen, 00-4959-52). Slides were imaged on a Leica TCS SP8 confocal microscope. Images were acquired at the lesion site, as well as rostral and caudal to the lesion site using the  $20\times$  objective with water immersion at  $1024\times 1024$  resolution.

### **Cell counts**

Images were relabelled to remove any group identifiers prior to analysis to ensure analyses were completed by a blinded observer. In Fiji is Just ImageJ (FIJI; v2.14.0), a maximum intensity projection of z-stacks were taken and then filtered using Gaussian blur (0.5) and then background subtracted (50 pixels). Microglia/macrophages were manually counted using FIJI. Cell nuclei were identified using DAPI, and colocalized to ensure a positive cell body. Each animal was counted as an independent  $n$ . Region of interests were identified in the lesion epicentre, and rostral and caudal to the lesion site, in the dorsal white matter, grey matter and ventral white matter. Cells were counted over the area of analysis to generate a cell density measurement.

### **Statistics**

For cell density measurements we used a two-way ANOVA, with a post hoc Tukey test identifying differences between the groups. All statistical analyses were performed using GraphPad Prism (v10).

### **Single-cell RNA sequencing and fluorescence-activated cell sorting**

Rats were euthanized with 1 mL of Euthanyl injected intraperitoneally, and then transcardially perfused with

Hanks' Balanced Salt Solution (HBSS, ThermoFisher, 14,175–103). All spinal cords were dissected and a 2 cm section surrounding the lesion site was isolated within 90 min after perfusion and maintained on ice for the duration of the cell sorting experiment. Spinal cords were diced in HBSS and then collected and placed into Dulbecco's Modified Eagle Medium (DMEM, Gibco, 11,960,069) and deoxyribonuclease (5 µg/mL, Worthington, L3002007). Collected tissue was mechanically dissociated and dounced 5 times with a loose-fitted dounce homogenizer; following which the suspension was passed through 70 µm and 40 µm filters (Cedarlane, 15-1070-1, 15-1040-1). Cells were then pelleted, resuspended in 5.4 mL of HBSS and myelin debris was removed using 1800 µl of Debris Removal Solution (Miltenyl Biotec, 130-109-398) and centrifugation at 3000 G for 10 min. The myelin debris was removed and cells were topped up to 15 mL with HBSS and centrifuged at 1000 G for 10 min. Cells were passed through a 20 µm filter (pluriS-trainger, 43-50,020-03), following which cells were resuspended in Fc block Anti-Mo CD16/CD32 (1:200, Invitrogen, 14-0161-85) blocking solution for 5 min, and subsequently stained with ZombieAqua (1:50, Biolegend, 423,101), DRAQ5 (1:1000, ThermoFisher, 62,240) and Cd11b (1:50, BD BioSciences, 561,684) for 20 min. Cells were resuspended in a solution of 1% bovine serum albumin (BSA; Sigma-Aldrich, A8806) dissolved in HBSS and then were isolated using fluorescence-activated cell sorting (FACS) on a Sony MA700 and gated for live, nucleated and Cd11b+ cells. Following sorting, cells were manually counted using a hemocytometer, pelleted and resuspended in HBSS.

### Library preparation

The FACS-isolated cells were processed using the 10×Genomics Chromium Next GEM Single Cell 3' GEM, Library and Gel Bead Kit v3.1 (10×Genomics; 1,000,121) and sequenced on the Illumina HiSeq P150 Sequencer (Novogene). The samples were paired-end, single index sequenced to an average of 40,000 reads per cell. The BCL file was demultiplexed to a FASTQ file and aligned to a custom *Rattus norvegicus* (6.0) reference genome manually annotated to include *Clec7a*, a polymorphic pseudogene. The samples were aligned to the genome with the count function from the 10×cell ranger pipeline (v3.0.0) to generate barcoded and sparse matrices.

### Quality control and clustering

First, ambient RNA was removed using CellBender [54]. Quality control was completed using the Seurat package (v4.3.0; [55]) in the R statistical environment (v4.2.2). Data were loaded into the R environment as a Seurat

object using the CreateSeuratObject with a minimum number of 3 cells and 200 features. Quality control was completed using the subset() function to remove doublets (greater than 4500 feature counts per cell) and dead or dying cells (mitochondrial gene percentage greater than 10%). The libraries were combined using the merge() function. The object was then normalized using the SCTransform() function with the vars.to.regress() function set to the mitochondrial percentage and the total number of molecules per cell. Subsequently, principal component analysis was performed (runPCA()). The number of PC was chosen based on the Elbow Plot, and FindNeighbours(dims=18) was run. The FindClusters() function was run and the object was exported as a h5ad object using SaveH5Seurat() and Convert(dest="h5ad") using the SeuratDisk (v0.0.0.9020) package. To complete unsupervised clustering analysis, we used the Single-Cell Clustering Assessment Framework (SCCAF; v0.0.10; [56]) in the Python environment (v3.9.13) opened in Jupyterlab (v3.4.4). SCCAF utilizes iterative machine learning to identify cell states until a self-projection accuracy of at least 90% was reached. An over-clustered resolution was set, and then SCCAF\_optimize\_all() was used to identify clusters. The final clustering was projected onto a UMAP using the sc.pl.umap() function using the scanpy module (v1.4.6).

### GO terms

Functional Gene Ontology (GO) Terms was used to examine the putative functional correlations of cell states. The top differentially expressed genes (DEGs) were identified for each cluster using the FindAllMarker() function in Seurat (min.pct=0.25, logfc.threshold=0.25). Mitochondrial and ribosomal genes were removed and the top DEGs for each cluster were utilized in the gProfiler web server (<https://biit.cs.ut.ee/gprofiler/>; [57]). The functional GO terms were then examined for each cluster, specifically from the GO (molecular function, biological process, cell component) and biological pathways (KEGG and Reactome) data sources. Terms of interest were retained and placed onto an alluvial plot using the ggplot(geom\_alluvial) function in the ggplot2 (v3.5.0) and ggalluvial (v0.12.5).

### Metabolic landscape

The Metabolic Landscape [58] pipeline was used to examine the metabolic pathways associated with the microglial responses after injury. Data were normalized using scan deconvolution using quickCluster() and calculateSumFactors() functions (v1.26.2; [59]), and then missing data were imputed using MAGIC imputation using the magic() function (v2.0.3; [60]). The genes associated with the metabolic pathways were taken from

KEGG metabolism database. The normalized deconvoluted data was inputted and the ratio of gene expression across all genes in a metabolic pathway was recorded and compared between clusters.

### Compass

The Compass algorithm (v0.9.10.2; [61]) was used to explore the potential activity of microglial metabolic reactions. Compass uses constraint-based optimization to model metabolic flux, considering the maximal metabolic flux possible, and then using the mRNA present catalyzing the reaction across multiple reactions and cells to infer the potential metabolic activity. The expression matrix, genes and sample names were inputted as tsv files and the program was run with the command `compass()` in the command line.

### CellChat

The R program CellChat [62] was used to predict cell–cell interactions. A custom CellChatDB was created featuring conversions of mouse genes to rat homologs. A merged file with normalized microglial cells and neuronal populations were merged and used to create an object within CellChat (`createCellChat`). The neuronal population was taken from ([63] GSE168156), using results obtained from single-nucleus RNA sequencing of the ventral tegmental area in naive female Sprague–Dawley rats between 90 and 120 days old. The overexpressed genes and receptor-ligands were examined using the `identifyOverExpressedGenes()` and `identifyOverExpressedInteractions()` functions. We used the `computeCommunProb()` function to examine the communication probability and infer the cellular communication network. Any cell–cell communication less than 10 cells was filtered using `filterCommunication()` function. The `computeCommunProbPathway()` function was used to examine the cell–cell communications at the pathway level. The `netVisual_chord_gene()` function was used to visualize the contributions of microglial inputs onto neuronal populations.

### RNA velocity

The programs scVelo (v0.2.2) and CellRank (v2.0.0) were both used to compute RNA velocity [64, 65]. Within scVelo, the data was normalized using `scv.pp.filter_and_normalize()`. The spliced and unspliced RNA dynamics were called with the `scv.tl.recover_dynamics()` function and the RNA velocity computed with the `scv.tl.velocity()` function, using the stochastic mode. The resulting velocity vectors were projected onto the existing UMAP with the `scv.pl.velocity_embedding_stream()` function. In CellRank, the CytoTRACE kernel was imported and used to compute a transition matrix. This transition matrix was used with a GPCCA estimator, using `compute_shur()` and `plot_spectrum()` functions to compute macrostates (`compute_macrostates()`) and predict initial (`predict_initial_states()`) and (`predict_terminal_states()`) terminal states.

## Results

### Microglial transcriptomic profiles shift from subacute to chronic SCI

The link between inflammation and training efficacy is supported by the work of Torres-Espin and colleagues, who demonstrate that inducing an inflammatory stimulus promotes higher training efficacy in the chronic stage after SCI, extending or reopening the window of opportunity for effective motor training. To characterize the subacute and chronic immune response corresponding to differences in training efficacy, we examined how microglial states changed with time and how an inflammatory stimulus that boosts training efficacy in female rats [11] altered the microglial responses in the chronic stage. We used scRNAseq on the spinal cords of female rats at a subacute stage (8 days post-injury [dpi]), as well as at a chronic stage (60 dpi) with either a sham saline injection (ChSaline) or an injection of LPS (ChLPS) to induce an inflammatory stimulus, as by Torres-Espin and colleagues ([11]; Fig. 1A). As described in the Methods, our experimental pipeline is illustrated in Fig. 1A and our quality control in Supp Fig. 1. We identified microglia

(See figure on next page.)

**Fig. 1** Microglia exhibit transcriptomic differences in subacute and chronic SCI, and with an LPS injection. **A** Schematic describing the experimental workflow and timeline. Female rats underwent a cervical SCI and animals were perfused, their spinal cords extracted, cold dissociated into a single cell suspension, sorted using Cd11b and then sequenced. **B** Microglia from the different libraries projected onto a UMAP, including 3,415 microglia from naïve animals, 14,767 from rats with subacute SCI, 1,188 from rats with chronic SCI and a saline injection (ChSaline), and 8,970 from rats with chronic SCI and an LPS injection (ChLPS). **C** Microglia (28,340) were clustered using Seurat and SCCAF, projected onto a UMAP and manually annotated. **D** Top DEGs for the different clusters. Homeostatic microglia are defined by the upregulation of canonical microglial genes (*P2ry12*, *Cx3cr1*), primed microglia by the expression of ribosomal genes (*Rps29* and *Rpl17*), myelin transcript-enriched microglia (MTEM) by the presence of transcripts from other cell types (*Plp1* and *Gfap*), DAM by the expression of *Lgals3*, *Apoe* and distinguished based on the presence of *Spp1* (*Spp1*-DAM) and complement genes (Complement-DAM), *Ccl3/4*-microglia express *Ccl3* and *Ccl4*, IRM express *Ifit2* and *Ifit3*, and proliferative microglia express *Mki67* and *Birc5*. Clusters of TM express a mixed phenotype between two microglial states. **E** The raw cell counts that make up each of the microglial clusters across the libraries. **F** Cells were downsampled to 1,188 cells and expressed as a percentage making up each cluster



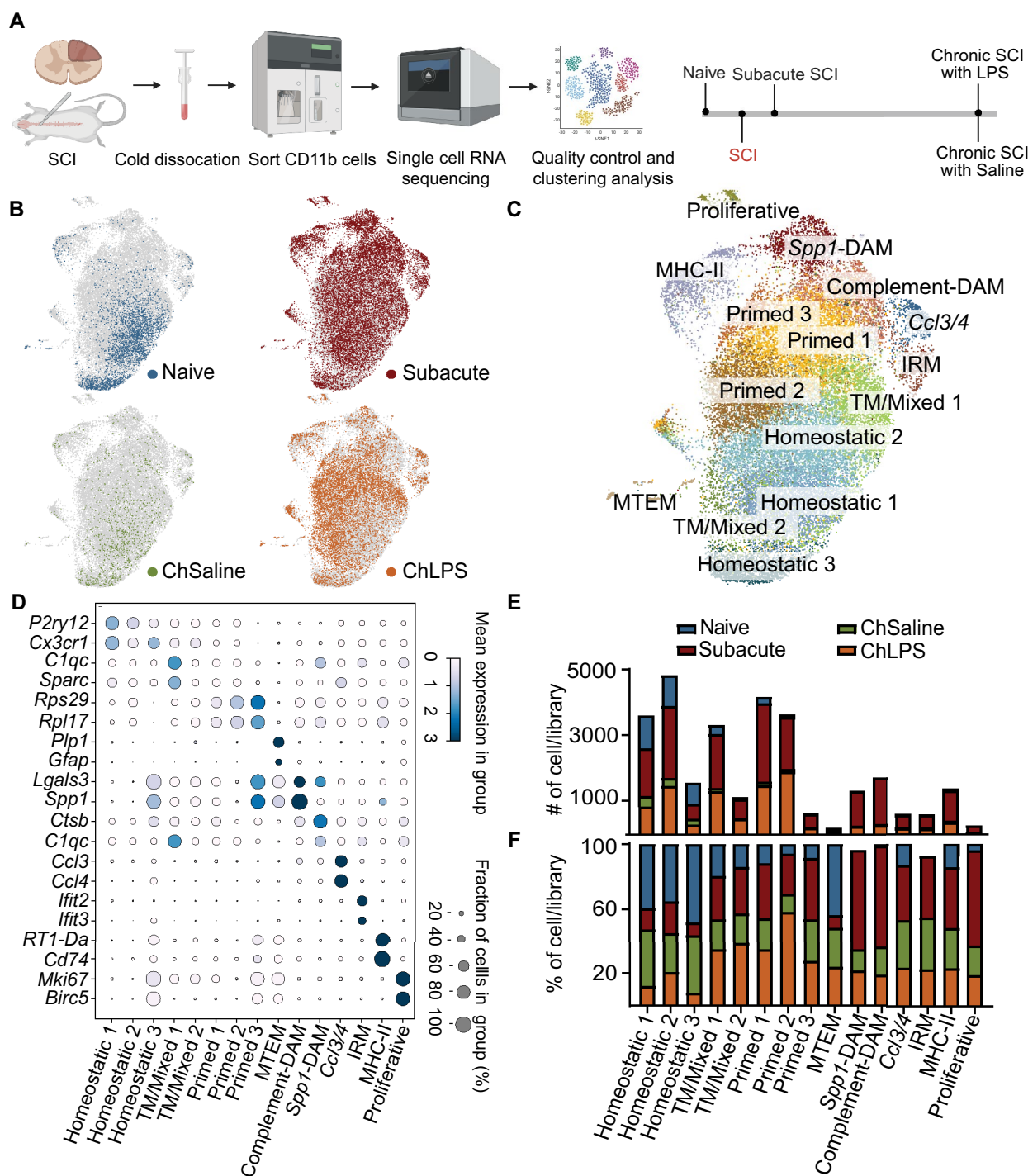


**Fig. 1** (See legend on previous page.)

using *P2ry12*, *Hexb* and *Tmem119*, as well as populations of border-associated macrophages (BAMs), monocytes, neutrophils, oligodendrocytes, and oligodendrocyte progenitor cells (OPCs; Supp Fig. 2). We reclustered and examined different subsets of BAMs (Supp Fig. 3),

monocytes (Supp Fig. 4), and neutrophils (Supp Fig. 5), as well as microglia. We obtained 28,340 microglia across our dataset, with 3,415 microglia from naïve animals, 14,767 from animals with a subacute injury, 1,188 from ChSaline animals and 8,970 from ChLPS animals.

To examine microglial states, we isolated microglia based on this initial clustering and reclustered the cells. Microglia from each library were projected onto a UMAP (Fig. 1B), demonstrating dramatic difference in the microglial states at different stages after SCI. Overall, we identified 14 clusters and used the differentially expressed genes (DEGs) to manually annotate these clusters (Fig. 1C). We identified three homeostatic clusters, based on the expression of canonical homeostatic microglial genes, including *P2ry12* and *Cx3cr1* ([66]; Fig. 1D). We also identified three primed states, which were enriched in ribosomal genes, including *Rps29* and *Rpl17* suggestive of heightened translation, resembling a microglial state observed in aged white matter [67] that contains a genetic signature globally increased in microglia in the aged brain ([68]; Fig. 1D). We further observed a range of injury-induced states, including two clusters that bore transcriptomic signatures similar to that observed in the disease-associated microglia (DAM) state [40, 45, 69], which was enriched in *Lgals3*, *Apoe* and *Igf1*. We further distinguished these DAM clusters based on enrichment in *Spp1* (*Spp1*-DAM) or complement genes (including *C1qc*; Complement-DAM). Other injury-induced clusters included one enriched in major histocompatibility complex II related genes (MHC-II), including *RT1-Da* and *Cd74*, while another cluster was enriched in chemokines *Ccl3* and *Ccl4* (*Ccl3/4*). We also identified a proliferative microglia cluster expressing *Mki67* and *Birc5* and an interferon-responsive microglial (IRM) state enriched in genes responding to interferons (including *Ifit2* and *Ifit3*). Those microglia identified with a mixed phenotype were termed Transitioning Microglia (TM/Mixed Microglia). Finally, we observed one small cluster of microglia that contain transcripts specific to other glial cells, including *Plp1* and *Gfap*, we refer to as Myelin Transcript-Enriched Microglia (MTEM). Despite quality control to remove multiplet cells and ambient RNA, we identified oligodendrocyte and astrocyte-specific transcripts within MTEM, which is similar to a state previously identified in an animal model of Alzheimer's Disease [70]. Overall, we identified several microglial states that occur after SCI.

Given the various states of microglia after SCI, we then sought to understand how these states changed with time after injury, as well as with an inflammatory stimulus at the chronic stage. Here, we evaluated each microglial states across each experimental condition, or library (Fig. 1E, F). We hypothesized that microglia would recapitulate the states observed after subacute injury after LPS injection in chronic SCI, which could point towards a microglial state associated with promoting neuroplasticity. We determined both the total number of cells (Fig. 1E) and the percentage of cells after normalization for each library (Fig. 1F) across each microglial cluster.

The majority of microglia from uninjured (naïve) rats, or 76% of microglia, were within homeostatic clusters (Fig. 1C). By contrast, microglia from subacute injured rats shifted away from homeostatic states (13.5% of microglia in homeostatic clusters) into injury-induced states. Microglia from subacute injured rats made up 61.6% of the *Spp1*-DAMs, 62.9% of the Complement-DAMs, 37.7% of IRMs, 37.5% of MHC-II-expressing microglia, 33.9% of *Ccl3/4*-expressing microglia, and 58.7% of proliferative microglia (Fig. 1C, E).

Chronic SCI is thought to be characterized by a stabilization of inflammatory processes [16]. To our surprise, ChSaline microglia were present in the same clusters as subacute SCI microglia, but at times at reduced levels, making up 15.2% of DAM clusters, 29.2% of *Ccl3/4*-microglia, 32.0% of IRM, 24.8% of MHC-II-microglia and 18.2% of proliferative microglia. At the same time, more ChSaline microglia shifted back towards a homeostatic state (32.1% of microglia from the ChSaline group compared to 13.5% in the subacute group). Overall, chronic SCI was characterized by a diverse microglial response, with a smaller proportion expressing signatures reminiscent of injury-induced microglial states compared to during the subacute phase.

Considering the microglial responses in chronic SCI, we were then interested in understanding how an inflammatory stimulus changes the microglial profile in the chronic phase of injury. Originally, we predicted that LPS injection would promote a more subacute SCI microglial response. However, in the ChLPS rats, microglia shifted away from the homeostatic states (13.6% of microglia from the ChLPS group compared to 32.1% from the ChSaline group) towards primed microglial states (40.2% of microglia from primed clusters in the ChLPS group compared to 19.1% from the ChSaline group). Additionally, microglia from the ChLPS group were more abundant in DAM clusters as compared to microglia from the ChSaline group, 20.3% compared to 15.2%, respectively (Fig. 1D–F). Systemic LPS injection, therefore, changed the microglial transcriptomic profiles, but LPS did not fully recapitulate the microglial responses observed during subacute injury. Taken together, our results suggest that subacute SCI was characterized by microglia shifting from a homeostatic signature to several diverse injury-induced states. Chronic SCI microglia were similarly diverse, with a reduction in these injury-induced states. Systemic LPS shifted microglia toward a primed state, although there was overlap in some states between subacute and chronic SCI with an LPS injection.

### Microglial trajectory after SCI

As microglia are highly adaptable to their environment and show plasticity in their cell states, we then explored

how microglia transition within our dataset. To do so, we utilized scVelo, which uses splicing dynamics across genes to infer the states with more active transcription (i.e., transitory) as compared to the states with less active transcription (i.e., terminal; [64, 65]). Splicing dynamics includes the presence of introns in nascent, or transitory, RNA and their absence in mature RNA. ScVelo identified several terminal states, including a range of injury-induced states, including DAM, IRM, MHC-II-microglia and proliferative microglia (Fig. 2A, B). Some microglia transitioned towards a homeostatic state. Relevant to microglia from LPS-treated rats, the primed microglial state was a key intermediary state, with trajectories both towards injury-induced and homeostatic clusters. Microglia after SCI, therefore, likely followed a complex series of transitions towards distinct injury induced states, with the potential to resolve toward a homeostatic microglial state. Injection of LPS promoted a primed microglial state, which was likely a key intermediate state.

#### **Microglial metabolic activity shifts in subacute SCI were incompletely resolved in chronic SCI**

Alongside the transcriptomic plasticity that microglia exhibit, changes in the environmental milieu also change the metabolic properties of microglia [71]. Given the complex environmental changes that underlie the transition from subacute to chronic SCI, we examined the metabolic pathway activity of microglia in our scRNAseq dataset. We utilized two different pipelines to explore the metabolic activity and heterogeneity across our datasets: Compass (Fig. 2C–E; [61]) and Metabolic Landscape (Fig. 2F, G, E; [58]). Compass models metabolic flux through constraint-based optimization and assigns a reaction score based on the presence of mRNA encoding enzymes catalyzing the reaction [61]. In microglia from the subacute phase, Compass analyses found increased energy metabolism, including glycolysis, the citric acid cycle, oxidative phosphorylation, and fatty acid oxidation compared to baseline (Fig. 2C), ChSaline (Fig. 2D) or ChLPS (Fig. 2E). The metabolic landscape pipeline uses the relative expression of genes expressed across 85 KEGG pathways to examine a pathway activity score that can be compared across the different libraries [58]. Metabolic Landscape analyses supported high levels of energy metabolism in subacute injury (Fig. 2F), and suggested the increased metabolic pathways were largely due to high levels within DAM and proliferative microglia (Fig. 2G). In the ChSaline animals, these same metabolic pathways remained elevated above the level observed in uninjured animals (Fig. 2D). However, unexpectedly, microglia from ChLPS animals exhibited decreases in energetic metabolic pathways to levels below uninjured animals (Fig. 2E). However, the metabolic landscape

analysis differed, instead showing a slight upregulation of energy metabolism after LPS administration compared to naïve animals, although at much lower levels than subacute injury (Fig. 2F). The metabolic activity following LPS administration in chronic SCI was likely due to more primed microglia, which were less metabolically active compared to DAM and proliferative states (Fig. 2G). Together, these analyses suggested that microglial metabolic activity was increased in subacute SCI, and decreased in chronic SCI, while systemic inflammation did not recapitulate the metabolic activity observed in the subacute phase.

Chondroitin sulfate proteoglycans (CSPGs) consist of two main components: the core protein and an inhibitory glycosaminoglycan chain. Digesting chondroitin sulfate glycosaminoglycan (GAG) chains with chondroitinase ABC facilitates plasticity and functional recovery following SCI [72–74]. Microglia can also digest both the CSPG-GAG chains in the CNS [75–77] and the core proteins [76] which may be one strategy for microglia to promote plasticity. We, therefore, examined the microglial metabolic pathways of GAG degradation. Microglia from subacute injury upregulated genes related to GAG degradation (Fig. 2F). The degradation of CSPGs remained elevated above baseline levels within ChSaline microglia (Fig. 2D). Microglia from ChLPS animals downregulated GAG biosynthesis pathways, although expressed GAG degradation genes at levels similar to baseline (Fig. 2E, F). Thus, GAG degradation may be a mechanism underlying the enhanced plasticity in the subacute period, which declines into the chronic period and was not restored by an LPS injection. Together, this data suggested that microglia globally shift their metabolic pathways subacutely after SCI, which remained elevated above baseline chronically. Broadly, systemic chronic LPS injection dampens microglial metabolic activity.

#### **Microglial-neuronal signalling shifts from subacute to chronic SCI**

Microglia exhibit complex interactions with other cell types in SCI, including astrocytes, B cells, endothelial cells and neurons [30, 35, 78, 79], which could change over time after SCI. Given the capability of microglia to respond to neuronal signalling [80] and modulate neuronal circuits and synaptic plasticity [81–83], we explored cell–cell interactions between microglia and the neurons from an external dataset. We utilized a dataset that included cortical neurons from the ventral tegmental area in young, female, uninjured rats [63]. With microglia from this study, we compared the microglial ligands that potentially regulate these cortical neurons with CellChat. CellChat uses a manually curated database of receptor-ligand interactions and



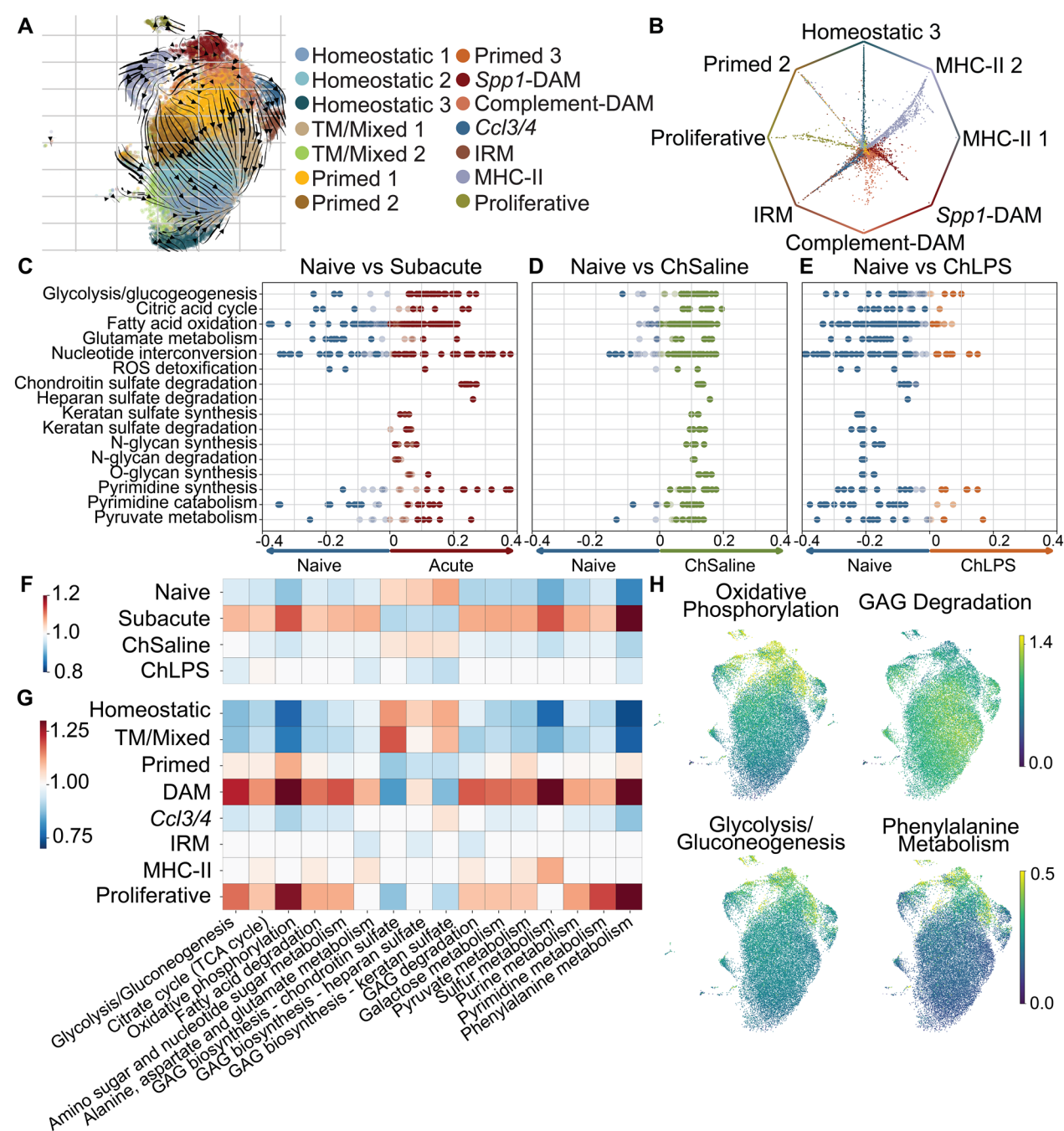


**Fig. 2** Microglia shift from primed to injury-induced and homeostatic states. **A** Microglial trajectories identified by scVelo based on the presence of unspliced and spliced RNA. **B** A plot showing terminal states identified by CellRank kernel. The terminal states are observed on the outside of the plot and the initial, transitioning states are observed on the inside of the plot. Microglial metabolic pathways identified by the Compass pipeline from the **(C)** subacute, **(D)** ChSaline, and **(E)** ChLPS microglia compared to microglia from naive, uninjured spinal cords. Reactions are defined by Recon2 pathways and the transparency of the dot represents the statistical significance. A Wilcoxon rank sum test was used to test between the groups and a Cohen's d statistic is computed for each reaction. The metabolic activity in the different **(F)** libraries and **(G)** clusters as identified by the Metabolic Landscape pipeline. Scores are a ratio, in which 1.0 represents mean activity for the microglial activity, scores above this represent upregulation in those groups and scores below represent downregulated groups. **H** The expression of genes in the metabolic pathways identified in **(F, G)** projected onto a UMAP

uses an algorithm that takes into account the overexpression of genes to predict interactions between cell types [62]. After SCI, there was an increase in microglial expressed Granulin (*Grn*) ligands, which bind to the Sortilin (*Sort1*) receptor expressed by neurons (Fig. 3A). Intriguingly, *Grn* encodes for Progranulin, a neurotrophic growth factor implicated in cell survival, lysosomal activity [84] and neurite outgrowth [85] and is upregulated following SCI [86, 87]. The *Grn*-*Sort1* interaction was prominent across all timepoints and present with all microglial states (Fig. 3B). We also identified microglial expressed Insulin-like growth factor 1 (*Igf1*) to neuronal expressed Insulin-like growth factor 1 receptor (*Igf1r*) interaction as an injury-specific receptor ligand pair (Fig. 3A). The probability

of interactions between *Igf1* and *Igf1r* increased with subacute and chronic injury, predominantly driven by DAM and proliferative microglia (Fig. 3B). Although *Igf1*-*Igf1r* signaling was also present in chronic SCI, it was reduced compared to subacute SCI, which could be a potential mechanism underlying the improved training efficacy in the subacute period, as *Igf1* is associated with corticospinal neuron sprouting in the injured cord [88, 89]. Cell signaling pathways associated with cell adhesion molecules were also upregulated following SCI, including *Cadm1*, *Jam2* and *F11r* onto *Cadm1* and *Jam3*, respectively (Fig. 3A). We projected *Grn*, *Igf1*, and *Cadm1* onto the UMAP and observed high localization of these genes to injury-induced states (Fig. 3C). Taken together, microglia-neuronal signaling was

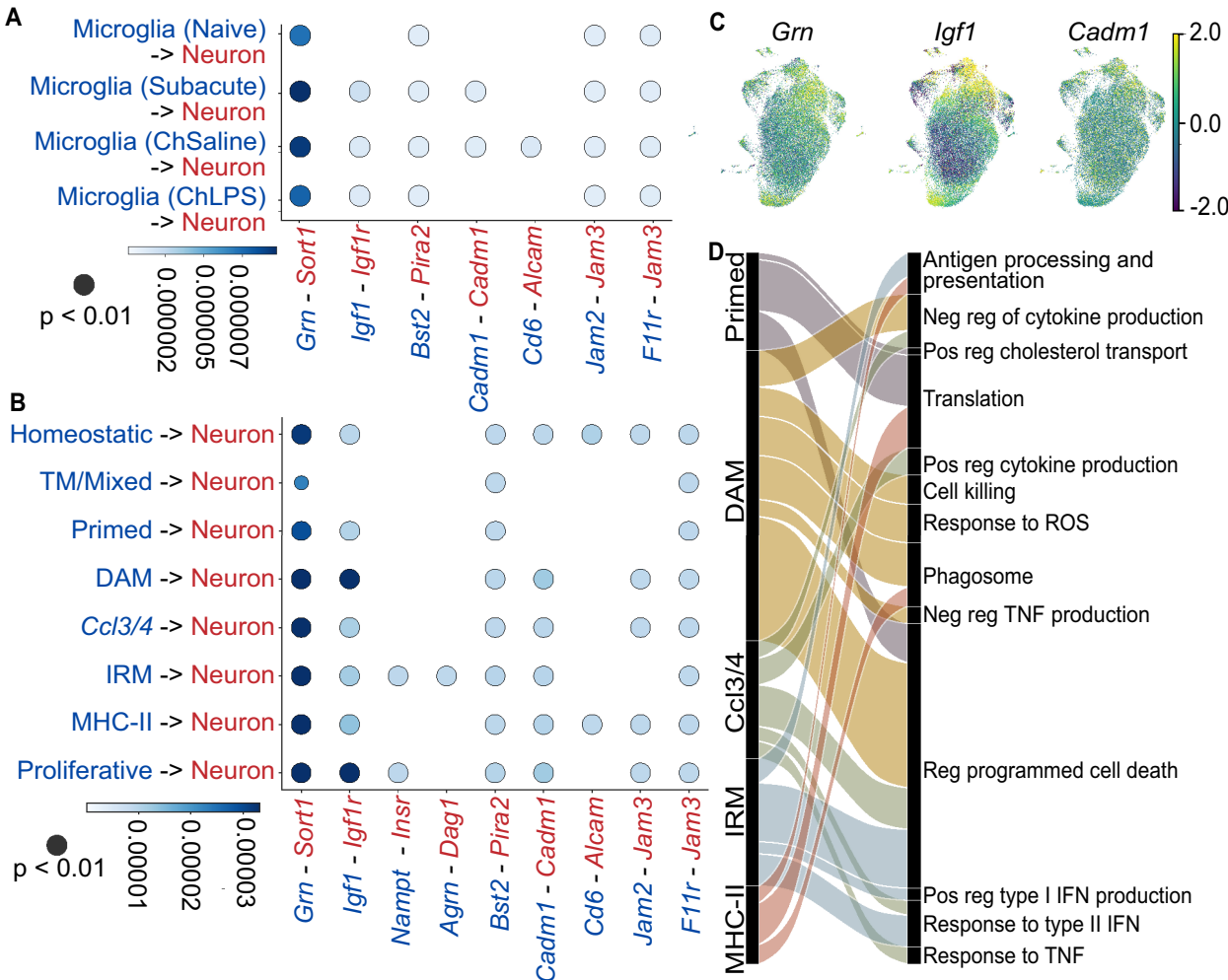


**Fig. 3** Interactions between microglia and neurons shift from subacute to chronic SCI. Significant predicted CellChat interactions between microglia (blue) and neurons (red) at the (A) library and (B) cluster level. More probable interactions are a darker hue. C The genes encoding the predicted microglial ligands projected onto a UMAP. D An alluvial plot showing key GO terms associated with each of the different microglial clusters

altered by SCI, and underwent transitions from subacute to chronic injury, although LPS injection did not appear to recapitulate the subacute pathways.

### Systemic inflammatory stimulus boosts DAM caudal to injury

To gain insight into the functional significance of diverse microglial states after SCI, we used Gene Ontology (GO) terms from gProfiler [57]. Primed microglia, enriched in chronic SCI with an LPS injection, were associated with translation, while DAM, enriched in subacute SCI, were associated with regulating cell death, responding to reactive oxygen species (ROS), phagocytosis and regulating cytokine production (Fig. 3D). The *Ccl3/4*-microglia were associated with similar predicted functional roles, including cytokine production regulation, regulating programmed cell death and response to TNF and type II interferon. The IRM, similarly, had predicted roles in both regulating type I interferon production and responding to type II interferon, while MHC-II-microglia had predicted roles in antigen processing and presentation, in translation, and in phagocytosis (Fig. 3D). Overall, these data point towards distinct putative roles for different microglial states after SCI, which, given the changes seen in microglial signatures with time after SCI, could underlie changes in function from the subacute to chronic phases after injury.

Given the predicted functional roles for the different microglial states, we then explored the spatial localizations of microglia with respect to the lesion site, in order to understand how these functional roles may be at play in the injured cord. We utilized Iba1 (a marker of microglia and macrophages) alongside either Galectin-3 (Gal3; a marker of DAM) or Cd74 (a marker of MHC-II-microglia). We evaluated microglia either at the lesion centre (Supp Fig. 6), rostral (Supp Fig. 7), or caudal to the injury site within dorsal white matter (Fig. 4). As expected, we observed a higher density of Iba1 staining at the lesion site of animals that sustained an injury, compared to naive controls (Supp Fig. 6). Examining the tissue rostral (Supp Fig. 7) and caudal (Fig. 4) to the injury site, Iba1+ densities were increased above baseline levels after chronic SCI, with or without an LPS injection, suggesting that microglial densities were increased in degenerated tracts in chronic SCI. Caudal to the injury site, LPS injection further boosted microglia/macrophage density compared to in chronic SCI alone (Fig. 4A–B). Given that LPS increased microglia density caudally (Fig. 4B), but not rostrally (Supp Fig. 7), this likely suggests that the LPS-mediated increased microglia density may have specifically targeted degenerated tracts below the injury site. Brennan and colleagues observe that microglia promote maladaptive plasticity in autonomic circuitry caudal

to the injury site in a high thoracic injury, and a similar mechanism may be at play here promoting motor plasticity [90]. Interestingly, previous studies have observed increased sprouting of the CST above the lesion with an LPS injection [11], but did not explore the areas below the injury site.

We were intrigued by the localization of DAM, as they have been observed across a variety of SCI models [35, 40, 79] and were key drivers of metabolic activity (Fig. 2) and microglial-neuronal interactions (Fig. 3). Gal3 is the protein encoded by *Lgals3*, which is enriched in DAM (Fig. 1E), and co-labelling with Iba1 was used to demarcate the DAM population. In the lesion site, the vast majority of Iba1+ cells co-labelled with Gal3, suggesting they were DAM. These DAM were not present in uninjured animals (Supp Fig. 6) and were found at equivalent densities across injury groups, suggesting that DAM persist in the lesion site into the chronic stage after injury. Within degenerating tracts caudal to the injury site, we found more microglia and macrophage expressing Gal3+ within chronic animals, which was further augmented with LPS injection (Fig. 4A–C). In the dorsal white matter caudal to the injury site, the percentage of microglia/macrophages that expressed Gal3 was 1% in the naive animals, increased to 44.9% in subacute animals, further increased to 59.3% in ChSaline animals and increased to 76.7% in ChLPS animals, suggesting that LPS stimulates a DAM state in caudal degenerated tracts.

We also examined Cd74, which was enriched in the MHC-II-microglia in the scRNAseq dataset. We found these Cd74+Iba1+ cells were a smaller population than Gal3+Iba1+ and were largely restricted to the lesion site within injured rats (Supp Fig. 9). Altogether, we found that most lesional microglia and macrophages express the DAM marker Gal3, and that this population was heightened within degenerated tracts caudal to the injury site following LPS injection. As our GO terms suggested DAM were associated with phagocytosis, their presence in the degenerated tracts could suggest enhanced phagocytosis in these regions that is induced by LPS.

### Discussion

After SCI, training efficacy is high in the subacute period after injury, and declines in the chronic period when animals have plateaued in their recovery, suggesting a ‘window of opportunity’ for effective training. In our rehabilitative training model (single pellet reaching and grasping; [11]), training onset was examined as early as 4 days post-injury [8], and improvements in training efficacy plateaued by 5 weeks [91], which could be described as chronic phase. Inflammation may dictate this window of opportunity, although the mechanisms by which the immune system contributes to plasticity

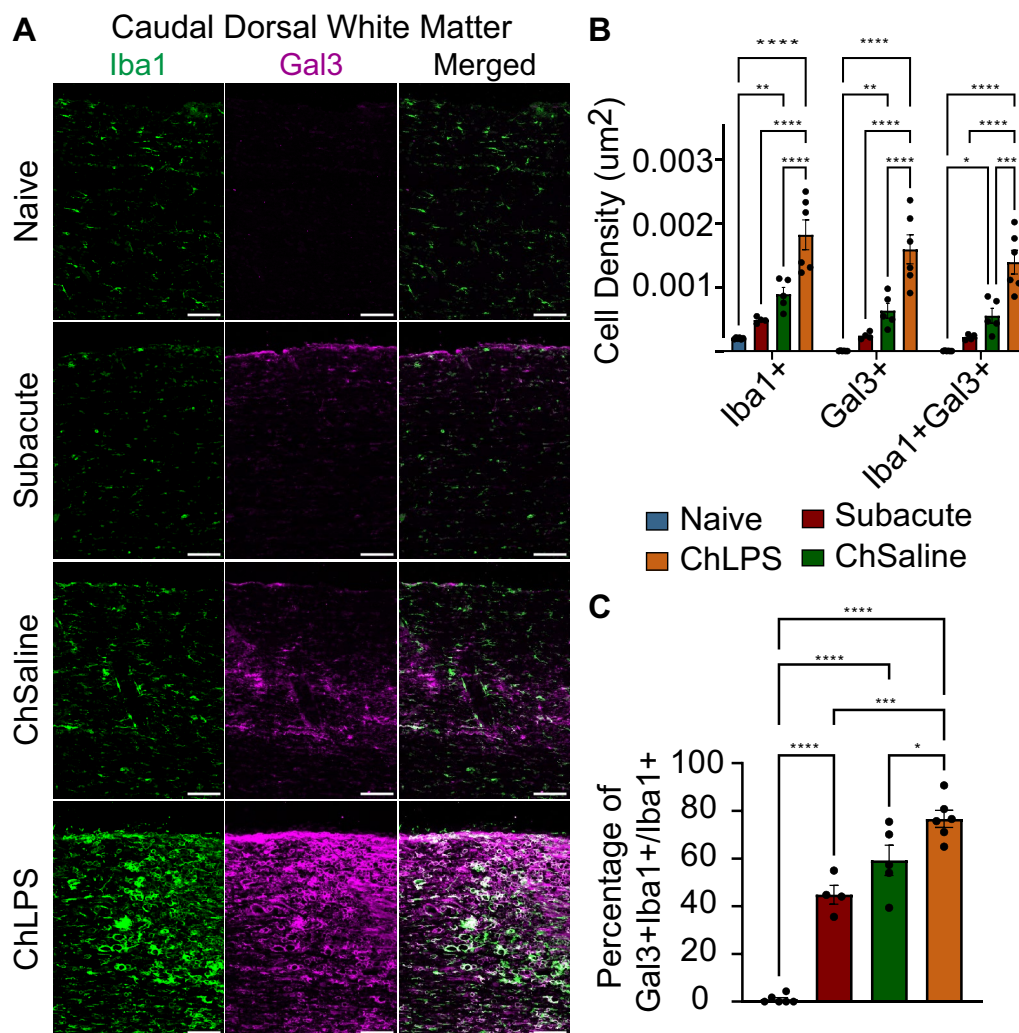


**Fig. 4** Injection of LPS augments DAM population in degenerated tracts caudal to the injury site. **A** Representative sagittal images of dorsal white matter caudal to the injury site in naive, subacute, ChSaline and ChLPS animals with Iba1 (green) labelling microglia and Gal3 (magenta) demarcating DAM (n=6 per group). **B** Quantification of the relative densities of Iba1+ cells, Gal3+ cells and colocalized cells. **C** The percentage of Iba1+ cells that also express Gal3+. Statistics run were a two-way ANOVA with a Tukey post hoc test. \*p<0.05, \*\*p<0.01, \*\*\*p<0.001, \*\*\*\*p<0.0001. Mean and SEM are represented on graphs

after injury is not yet fully elucidated. Here, we used scRNAseq to examine the microglial response from subacute to chronic cervical SCI in rats. We found distinct microglial signatures, many of which overlapped between the subacute and chronic periods. The subacute period is hallmarked by a shift away from homeostatic microglial states and the establishment of a range of injury-induced states, predominantly proliferative and DAM states. The subacute period is also associated with an increase in energy metabolism and glycosaminoglycan degradation metabolic pathways, alongside *Igf1* signalling, which is decreased by the chronic phase after injury. Chronic SCI is characterized by a retained injury-induced signature, including IRM, MHC-II- and *Ccl3/4*-expressing

microglia, with more microglia expressing a homeostatic signature. Microglial transcriptomic signatures were altered by an injection of LPS in chronic injury, which shifts microglia towards a primed microglia state associated with elevated levels of translation related genes.

We found that the DAM states, in particular, were a strong candidate for the plasticity-inducing mechanisms that underlie microglial control of the window of opportunity. The DAM highly express *Igf1*, which is a predicted ligand for neurons and a known promoter of the glial scar formation [36]. The overexpression of *Igf1* is also associated with increased axon outgrowth in corticospinal tract neurons after SCI [81], which is sensitized by co-expression of *Spp1* [89], another



upregulated gene in the DAM population. The strength of *Igf1* receptor-ligands was highest in the subacute period, a time when training provides better outcomes [4, 8, 10, 11, 91, 92]. Additionally, *Spp1* overexpression in combination with rehabilitative training promoted outgrowth of CST neurons, further supporting a role for DAM genes in promoting plasticity [93].

We also identified an injury-related increased probability of microglial granulin interacting with neuronal sortilin receptor. Microglial granulin, which encodes for progranulin, has been shown to increase following SCI [86, 94]. Granulin may promote plasticity given *in vitro* work shows an improvement in neurite outgrowth in cultured neurons [85].

Another plasticity promoting mechanism we identified with our scRNAseq data is the regulation of extracellular matrix molecules. We found chondroitin sulphate, heparan sulfate, and glycosaminoglycan degradation was enriched within microglia during the subacute period. These changes are interesting because overall levels of the extracellular matrix molecule CSPGs are upregulated during the subacute period [95] and are associated with growth-inhibitory properties of the glial scar [15] and the distal regions of the spinal cord [95]. However, while microglia can produce the necessary components to contribute to inhibitory ECM molecules [96] after SCI, the predominant CSPG producing cells are astrocytes [97, 98], although oligodendrocytes, OPCs and neurons may also contribute [99, 100].

One major regulator of plasticity rich in CSPGs are perineuronal nets (PNN), which surround specific neuronal populations [101]. The degradation of CSPGs, some likely within PNN, enables axon growth after SCI [72, 73]. In both Alzheimer's and Huntington's mouse models, microglial depletion is sufficient to ameliorate disease-related PNN loss and microglial depletion in wild-type mice causes global PNN accumulation, suggesting microglia prune PNNs [75, 77]. CSPGs contain two structural components: a protein core and glycosaminoglycan (GAG) chains. Removal of GAG chains from CSPGs is sufficient to prevent much of their inhibitory activity [72, 73]. Therefore, the microglial breakdown of GAG, some potentially residing within PNN, may contribute to the enhanced plasticity in this period after injury. The DAM increased GAG degradation pathways more so than other microglial states after SCI, linking this state to enhancing plasticity. Microglial degradation of GAG is upregulated in the subacute period, which may implicate microglia in the regulation of CSPGs after injury, although additional experiments would be necessary to confirm this role. Our scRNAseq data points towards potential microglial roles in enabling plasticity in the subacute period, which could

contribute to the enhanced training efficacy observed during that phase.

An inflammatory stimulus administered in the chronic phase enables increased training efficacy [11, 19], although the mechanisms by which an inflammatory stimulus may influence plasticity in the CNS remain unclear. We initially hypothesized that LPS in a chronic setting would recapitulate the subacute injury response, when plasticity and training efficacy is heightened. Here, contrary to our hypothesis, we showed that microglia adopt a distinct signature after LPS injection to chronically injured rats. Schmidt and colleagues found LPS boosted functional recovery even in the highly inflammatory subacute period [102], which suggests that plasticity may be mediated differently by LPS-induced inflammation as opposed to the subacute inflammatory response to SCI. We found LPS injection induced a primed microglial state, which was highly enriched in translation-associated genes. Brennan and colleagues found a microglial state at 7 days following SCI that resembled the primed microglia enriched with an LPS injection [35]. Our RNA velocity analysis suggested the primed microglial state was transitory and would resolve into a range of injury-induced and homeostatic states, including DAM. Therefore, the primed microglial state induced by LPS injection could represent an activation trajectory that is present in the subacute period after SCI, which terminates into a range of injury-induced states. However, further work is needed to examine microglial dynamics at later time points after LPS injection to ascertain the evolution of microglial states.

Our work supports the continued presence of DAM in chronic SCI, albeit at reduced levels compared to subacute SCI. Interestingly, we identified an increased DAM population in the degenerated white matter tracts caudal to the injury in animals that had received an LPS injection. Given the upregulated phagocytic genes in the DAM state, DAM are postulated to clear debris [69, 70]. Indeed, we found GO terms identified phagocytosis as a probable role for DAM after SCI, although additional validation experiments would be necessary to confirm this. Debris remains in the injured cord in rats for at least 8 weeks following SCI [103] and for years in humans with a SCI [104] and the elevated DAM could be playing roles in removing this debris. In the subacute period, LPS injection increases myelin phagocytosis via microglia/macrophages expressing Gal3 in regions of Wallerian degeneration [105]. Similarly, LPS injection also increases lipid droplets within microglia in the chronically injured spinal cord several weeks following an LPS injection [19]. We found DAM markers within degenerating white matter tracts below the injury site. Of note, Fan

and colleagues utilized a collagen scaffold following a complete transection in rhesus monkeys and found an increased DAM population caudal to the injury site, as well as accompanying improvement in functional recovery, increases in myelination and increases in growth factor expression (79). The similar increases in DAM distal to the site of injury across different injury models could suggest a conserved microglial response.

The phagocytosis of myelin debris is implicated in improving the microenvironment after SCI, which could enable enhanced plasticity. After SCI, several myelin and oligodendrocyte-derived components exhibit growth inhibitory properties, including myelin-associated glycoprotein (MAG), oligodendrocyte myelin glycoprotein (OMgp) and Nogo-A, which is expressed by both oligodendrocytes and myelin, all of which contribute to regenerative failure of axons in the injured cord [106, 107]. Further, antibodies produced against the myelin-associated neurite inhibitors contribute to increased axonal sprouting and growth [74, 108–110]. Phagocytosis of existing myelin debris could facilitate a microenvironment more conducive to axonal sprouting. Delays in debris clearance following Wallerian degeneration in the central nervous system has been suggested to contribute to reduced regeneration compared to the peripheral nervous system [109]. Myelin phagocytosis is an important rate-limiting step during remyelination [111–113]. While remyelination may not be required for functional recovery after contusive SCI [114], it is observed alongside cell transplantation therapies that improve functional recovery [111, 115, 116], which may suggest a beneficial role in SCI. Cellular responses that promote remyelination likely also have other benefits. For example, metformin treatment after SCI regulates microglial autophagic flux, increasing myelin debris clearance and myelination, yet also increases axon growth [117]. Our data points towards a potential role of LPS in boosting microglial phagocytosis of myelin debris, which can contribute to an enhanced regenerative environment in the injured spinal cord. Importantly, while our data shows the shifts that occur in microglial transcriptomes across time after injury or with an inflammatory stimulus, it is limited in showing causative gain-of-function or loss-of-function roles of these microglial states, which would be an important future direction to confirm the hypothesized microglial roles. Our data highlights the changes in microglial states, although further work is necessary to understand how these changes contribute to the complex injury microenvironment, as well as how rehabilitation could interact and alter the environment in the chronically injured spinal cord.

## Conclusion

Here we find a shift in microglial transcriptomic profiles from the subacute to the chronic phases of SCI, which correlated with periods of high and low training efficacy, respectively. Microglia in subacute SCI were characterized by increases in proliferative microglia and DAM, which appear to be candidates for enabling plasticity in the subacute period after injury. The chronic phase of SCI was highly diverse, with similar injury-induced microglial states as present in the subacute period, albeit at decreased levels, and with a concomitant shift back to homeostatic microglial signatures. LPS injection in the chronic period after injury induces a primed microglial state that appears to be a transitory state, as well as boosts DAM in the degenerated tracts caudal to the injury site, which may enable improved debris clearance and improve the microenvironment for axon growth. Overall, we demonstrate that a diverse microglia response is initiated by SCI and persists chronically, with multiple mechanisms to boost plasticity, making microglia stimulating therapies attractive to enhance plasticity and boost recovery.

## Supplementary Information

The online version contains supplementary material available at <https://doi.org/10.1186/s12974-025-03379-6>.

**Supplementary material 1: Figure S1:** Quality control of the scRNAseq dataset, description of how quality control was completed. **Figure S2:** Clustering and identification of cell types present in the scRNAseq dataset, cell types identified in the scRNAseq dataset projected onto a UMAP and dotplot, as well as the score of ex vivo activation. **Figure S3:** BAM clusters observed in the scRNAseq dataset, BAM clusters projected onto a UMAP, across the different libraries and the top DEGs for each cluster. **Figure S4:** Monocyte clusters observed in the scRNAseq dataset, monocyte clusters projected onto a UMAP, across the different libraries and the top DEGs for each cluster. **Figure S5:** Neutrophil clusters identified in the scRNAseq dataset, neutrophil clusters projected onto a UMAP, across the different libraries and the top DEGs for each cluster. **Figure S6:** DAM predominate in the lesion site from subacute to chronic SCI, immunofluorescence images of Iba1 + and Gal3 + cells in the lesion site and corresponding quantifications. **Figure S7:** Microglia/macrophage density increased in the rostral dorsal white matter in chronic SCI, immunofluorescence images of Iba1 + and Gal3 + cells in the dorsal white matter rostral to the lesion site and corresponding quantifications. **Figure S8:** Microglia/macrophages densities do not change in the ventral white matter rostral and caudal to the injury site, immunofluorescence images of Iba1 + and Gal3 + cells in the ventral white matter rostral and caudal to the lesion site and corresponding quantifications. **Figure S9:** MHC-II-microglia/macrophages are not impacted by time after injury, immunofluorescence images of Iba1 + and Cd74 + cells in the lesion site and corresponding quantifications.

## Acknowledgements

We would like to thank the University of Alberta Faculty of Medicine & Dentistry Flow Cytometry Facility, the Advanced Cell Exploration Core, and the University of Alberta Health Sciences Lab Animal Services.

## Author contributions

Conceptualization: K.F. and J.R.P.; Methodology: R.K.J., S.Z., K.F. and J.R.P.; Formal Analysis: R.K.J., S.V., S.Z.; Investigation: R.K.J., S.P.V., S.Z., K.V.L., A.T.N., A.T., K.K.F.,

C.N., E.S., R.V., P.R., K.S., K.F. and J.R.P.; Writing – Original Draft: R.K.J., K.F., and J.R.P., Review & Editing: R.K.J., S.P.V., S.Z., K.V.L., A.T.N., A.T., K.F.F., C.N., E.S., R.V., P.R., K.S., K.F., and J.R.P.; Supervision: K.F. and J.R.P.; Funding Acquisition: J.R.P. and K.F.

### Funding

RKJ was funded by a master's CIHR fellowship. A master's NSERC fellowship funded SZ. This work was funded by operating grants held by KF from International Spinal Research Fund and the Christopher and Dana Reeve Foundation and JRP from CIHR. JRP and KF hold Canada Research Chairs.

### Availability of data and materials

The datasets supporting the conclusions of this article are available in the Gene Expression Omnibus, accession number GSE281996, link: <https://www.ncbi.nlm.nih.gov/geo/query/acc.cgi?acc=GSE281996>. The datasets generated during the current study are available in the Gene Expression Omnibus under accession number GSE281996.

### Declarations

#### Ethics approval and consent to participate

All animal studies were conducted in accordance with the Canadian Council on Animal Care Guidelines and Policies with approval from the Animal Care and Use Committee: Health Sciences for the University of Alberta under AUP #254.

#### Consent for publication

Not applicable.

#### Competing interests

The authors declare that they have no competing interests.

#### Author details

<sup>1</sup>Neuroscience and Mental Health Institute, University of Alberta, Edmonton, Canada. <sup>2</sup>Department of Physical Therapy, Faculty of Rehabilitation Medicine, University of Alberta, Edmonton, Canada. <sup>3</sup>Department of Medicine, Division of Neurology, University of Alberta, Edmonton, Canada. <sup>4</sup>Department of Medical Microbiology and Immunology, University of Alberta, Edmonton, Canada. <sup>5</sup>Li Ka Shing Institute of Virology, Faculty of Medicine and Dentistry, University of Alberta, Edmonton, Canada. <sup>6</sup>School of Public Health Sciences, Faculty of Health, University of Waterloo, Waterloo, Canada.

Received: 20 November 2024 Accepted: 14 February 2025

Published online: 28 February 2025

### References

- Dietz V, Harkema SJ. Locomotor activity in spinal cord-injured persons. *J Appl Physiol*. 2004;96(5):1954–60.
- Hubli M, Dietz V. The physiological basis of neurorehabilitation–locomotor training after spinal cord injury. *J Neuroeng Rehabil*. 2013;10:5.
- Fouad K, Tetzlaff W. Rehabilitative training and plasticity following spinal cord injury. *Exp Neurol*. 2012;235(1):91–9.
- Norrie BA, Nevett-Duchcherer JM, Gorassini MA. Reduced functional recovery by delaying motor training after spinal cord injury. *J Neurophysiol*. 2005;94(1):255–64.
- Maier IC, Baumann K, Thallmair M, Weinmann O, Scholl J, Schwab ME. Constraint-induced movement therapy in the adult rat after unilateral corticospinal tract injury. *J Neurosci*. 2008;28(38):9386–403.
- Sumida M, Fujimoto M, Tokuhira A, Tominaga T, Magara A, Uchida R. Early rehabilitation effect for traumatic spinal cord injury. *Arch Phys Med Rehabil*. 2001;82(3):391–5.
- Chen Q, Zhou L, Shine HD. Expression of neurotrophin-3 promotes axonal plasticity in the acute but not chronic injured spinal cord. *J Neurotrauma*. 2006;23(8):1254–60.
- Girgis J, Merrett D, Kirkland S, Metz GA, Verge V, Fouad K. Reaching training in rats with spinal cord injury promotes plasticity and task specific recovery. *Brain*. 2007;130(Pt 11):2993–3003.
- Faw TD, Lakhani B, Schmalbrock P, Knopp MV, Lohse KR, Kramer JLK, et al. Eccentric rehabilitation induces white matter plasticity and sensorimotor recovery in chronic spinal cord injury. *Exp Neurol*. 2021;346: 113853.
- Fenrich KK, Hallworth BW, Vavrek R, Raposo PJF, Misiaszek JE, Bennett DJ, et al. Self-directed rehabilitation training intensity thresholds for efficient recovery of skilled forelimb function in rats with cervical spinal cord injury. *Exp Neurol*. 2021;339: 113543.
- Torres-Espin A, Forero J, Fenrich KK, Lucas-Osma AM, Krajacic A, Schmidt E, et al. Eliciting inflammation enables successful rehabilitative training in chronic spinal cord injury. *Brain*. 2018;141(7):1946–62.
- Lewis NE, Tabarestani TQ, Cellini BR, Zhang N, Marrotte EJ, Wang H, et al. Effect of acute physical interventions on pathophysiology and recovery after spinal cord injury: a comprehensive review of the literature. *Neurospine*. 2022;19(3):671–86.
- Ahuja CS, Wilson JR, Nori S, Kotter MRN, Druschel C, Curt A, et al. Traumatic spinal cord injury. *Nat Rev Dis Primers*. 2017;3:17018.
- Dumont RJ, Okonkwo DO, Verma S, Hurlbert RJ, Boulous PT, Ellegala DB, et al. Acute spinal cord injury, part I: pathophysiologic mechanisms. *Clin Neuropharmacol*. 2001;24(5):254–64.
- Fawcett JW, Asher RA. The glial scar and central nervous system repair. *Brain Res Bull*. 1999;49(6):377–91.
- Beck KD, Nguyen HX, Galvan MD, Salazar DL, Woodruff TM, Anderson AJ. Quantitative analysis of cellular inflammation after traumatic spinal cord injury: evidence for a multiphasic inflammatory response in the acute to chronic environment. *Brain*. 2010;133(Pt 2):433–47.
- Ballermann M, Fouad K. Spontaneous locomotor recovery in spinal cord injured rats is accompanied by anatomical plasticity of reticulospinal fibers. *Eur J Neurosci*. 2006;23(8):1988–96.
- Chen Q, Smith GM, Shine HD. Immune activation is required for NT-3-induced axonal plasticity in chronic spinal cord injury. *Exp Neurol*. 2008;209(2):497–509.
- Zhong J, He Y, Zhao Q, Luo H, Zhang Q, Tian Y, et al. Low-dose LPS modulates microglia/macrophages phenotypic transformation to amplify rehabilitation effects in chronic spinal cord injured (CSCI) mice. *Mol Neurobiol*. 2024.
- Leon S, Yin Y, Nguyen J, Irwin N, Benowitz LI. Lens injury stimulates axon regeneration in the mature rat optic nerve. *J Neurosci*. 2000;20(12):4615–26.
- Fischer D, Pavlidis M, Thanos S. Cataractogenic lens injury prevents traumatic ganglion cell death and promotes axonal regeneration both in vivo and in culture. *Invest Ophthalmol Vis Sci*. 2000;41(12):3943–54.
- Fischer D, Hawk TG, Muller A, Thanos S. Crystallins of the beta/gamma-superfamily mimic the effects of lens injury and promote axon regeneration. *Mol Cell Neurosci*. 2008;37(3):471–9.
- Yin Y, Cui Q, Li Y, Irwin N, Fischer D, Harvey AR, et al. Macrophage-derived factors stimulate optic nerve regeneration. *J Neurosci*. 2003;23(6):2284–93.
- Yin Y, Henzl MT, Lorber B, Nakazawa T, Thomas TT, Jiang F, et al. Oncomodulin is a macrophage-derived signal for axon regeneration in retinal ganglion cells. *Nat Neurosci*. 2006;9(6):843–52.
- Yin Y, Cui Q, Gilbert HY, Yang Y, Yang Z, Berlinic C, et al. Oncomodulin links inflammation to optic nerve regeneration. *Proc Natl Acad Sci U S A*. 2009;106(46):19587–92.
- Kurimoto T, Yin Y, Habboub G, Gilbert HY, Li Y, Nakao S, et al. Neutrophils express oncomodulin and promote optic nerve regeneration. *J Neurosci*. 2013;33(37):14816–24.
- Leibinger M, Muller A, Gobrecht P, Diekmann H, Andreadaki A, Fischer D. Interleukin-6 contributes to CNS axon regeneration upon inflammatory stimulation. *Cell Death Dis*. 2013;4(4): e609.
- Leibinger M, Andreadaki A, Diekmann H, Fischer D. Neuronal STAT3 activation is essential for CNTF- and inflammatory stimulation-induced CNS axon regeneration. *Cell Death Dis*. 2013;4(9): e805.
- Fischer D. What are the principal mediators of optic nerve regeneration after inflammatory stimulation in the eye? *Proc Natl Acad Sci USA*. 2010;107(3):8.
- Freria CM, Hall JC, Wei P, Guan Z, McTigue DM, Popovich PG. Deletion of the fractalkine receptor, CX3CR1, improves endogenous repair, axon sprouting, and synaptogenesis after spinal cord injury in mice. *J Neurosci*. 2017;37(13):3568–87.
- Gris D, Marsh DR, Oatway MA, Chen Y, Hamilton EF, Dekaban GA, et al. Transient blockade of the CD11d/CD18 integrin reduces secondary

- damage after spinal cord injury, improving sensory, autonomic, and motor function. *J Neurosci*. 2004;24(16):4043–51.
32. Popovich PG, Guan Z, Wei P, Huitinga I, van Rooijen N, Stokes BT. Depletion of neurotogenic macrophages promotes partial hindlimb recovery and neuroanatomical repair after experimental spinal cord injury. *Exp Neurol*. 1999;158(2):351–65.
  33. Gensel JC, Nakamura S, Guan Z, van Rooijen N, Ankeny DP, Popovich PG. Macrophages promote axon regeneration with concurrent neurotoxicity. *J Neurosci*. 2009;29(12):3956–68.
  34. Kigerl KA, Gensel JC, Ankeny DP, Alexander JK, Donnelly DJ, Popovich PG. Identification of two distinct macrophage subsets with divergent effects causing either neurotoxicity or regeneration in the injured mouse spinal cord. *J Neurosci*. 2009;29(43):13435–44.
  35. Brennan FH, Li Y, Wang C, Ma A, Guo Q, Li Y, et al. Microglia coordinate cellular interactions during spinal cord repair in mice. *Nat Commun*. 2022;13(1):4096.
  36. Bellver-Landete V, Bretheau F, Mailhot B, Vallières N, Lessard M, Janelle ME, et al. Microglia are an essential component of the neuroprotective scar that forms after spinal cord injury. *Nat Commun*. 2019;10(1):518.
  37. Wang R, Hong J, Lu M, Neil JE, Vitek MP, Liu X, et al. ApoE mimetic ameliorates motor deficit and tissue damage in rat spinal cord injury. *J Neurosci Res*. 2014;92(7):884–92.
  38. Wang X, Cao K, Sun X, Chen Y, Duan Z, Sun L, et al. Macrophages in spinal cord injury: phenotypic and functional change from exposure to myelin debris. *Glia*. 2015;63(4):635–51.
  39. Fu H, Zhao Y, Hu D, Wang S, Yu T, Zhang L. Depletion of microglia exacerbates injury and impairs function recovery after spinal cord injury in mice. *Cell Death Dis*. 2020;11(7):528.
  40. Hakim R, Zachariadis V, Sankavaram SR, Han J, Harris RA, Brundin L, et al. Spinal cord injury induces permanent reprogramming of microglia into a disease-associated state which contributes to functional recovery. *J Neurosci*. 2021;41(40):8441–59.
  41. Paolicelli R, Sierra A, Stevens B, Tremblay M-E, Aguzzi A, Ajami B, et al. Defining microglial states and nomenclature: a roadmap to 2030. *Cell*. 2022;110:3458–83.
  42. Dolan MJ, Therrien M, Jereb S, Kamath T, Gazestani V, Atkeson T, et al. Exposure of iPSC-derived human microglia to brain substrates enables the generation and manipulation of diverse transcriptional states in vitro. *Nat Immunol*. 2023;24(8):1382–90.
  43. Friedman BA, Srinivasan K, Ayalon G, Meilandt WJ, Lin H, Huntley MA, et al. Diverse brain myeloid expression profiles reveal distinct microglial activation states and aspects of alzheimer's disease not evident in mouse models. *Cell Rep*. 2018;22(3):832–47.
  44. Hammond TR, Dufort C, Dissing-Olesen L, Giera S, Young A, Wysoker A, et al. Single-cell RNA sequencing of microglia throughout the mouse lifespan and in the injured brain reveals complex cell-state changes. *Immunity*. 2019;50(1):253–71.e6.
  45. Keren-Shaul H, Spinrad A, Weiner A, Matcovitch-Natan O, Dvir-Szternfeld R, Ulland TK, et al. A unique microglia type associated with restricting development of alzheimer's disease. *Cell*. 2017;169(7):1276–90.e17.
  46. Masuda T, Sankowski R, Staszewski O, Bottcher C, Amann L, Sagar N, et al. Spatial and temporal heterogeneity of mouse and human microglia at single-cell resolution. *Nature*. 2019;566(7744):388–92.
  47. Plemel JR, Stratton JA, Michaels NJ, Rawji KS, Zhang E, Sinha S, et al. Microglia response following acute demyelination is heterogeneous and limits infiltrating macrophage dispersion. *Sci Adv*. 2020;6(3):eaay6324.
  48. Tansley S, Uttam S, Urena Guzman A, Yaqubi M, Pacis A, Parisien M, et al. Single-cell RNA sequencing reveals time- and sex-specific responses of mouse spinal cord microglia to peripheral nerve injury and links ApoE to chronic pain. *Nat Commun*. 2022;13(1):843.
  49. Zia S, Hammond BP, Zirngibl M, Sizov A, Baaklini CS, Panda SP, et al. Single-cell microglial transcriptomics during demyelination defines a microglial state required for lytic carcass clearance. *Mol Neurodegener*. 2022;17(1):82.
  50. Matson KJE, Russ DE, Kathe C, Hua I, Maric D, Ding Y, et al. Single cell atlas of spinal cord injury in mice reveals a pro-regenerative signature in spinocerebellar neurons. *Nat Commun*. 2022;13(1):5628.
  51. Milich LM, Choi JS, Ryan C, Cerqueira SR, Benavides S, Yahn SL, et al. Single-cell analysis of the cellular heterogeneity and interactions in the injured mouse spinal cord. *J Exp Med*. 2021;218(8):e20210040.
  52. Wang J, Xu L, Lin W, Yao Y, Li H, Shen G, et al. Single-cell transcriptome analysis reveals the immune heterogeneity and the repopulation of microglia by Hif1alpha in mice after spinal cord injury. *Cell Death Dis*. 2022;13(5):432.
  53. Li Y, He X, Kawaguchi R, Zhang Y, Wang Q, Monavarfeshani A, et al. Microglia-organized scar-free spinal cord repair in neonatal mice. *Nature*. 2020;587(7835):613–8.
  54. Fleming SJ, Chaffin MD, Arduini A, Akkad AD, Banks E, Marioni JC, et al. Unsupervised removal of systematic background noise from droplet-based single-cell experiments using Cell Bender. *Nat Methods*. 2023;20(9):1323–35.
  55. Hao Y, Hao S, Andersen-Nissen E, Mauck WM, Zheng S, Butler A, et al. Integrated analysis of multimodal single-cell data. *Cell*. 2021;184(13):3573–87.e29.
  56. Miao Z, Moreno P, Huang N, Papatheodorou I, Brazma A, Teichmann SA. Putative cell type discovery from single-cell gene expression data. *Nat Methods*. 2020;17(6):621–8.
  57. Kolberg L, Raudvere U, Kuzmin I, Adler P, Vilo J, Peterson H. g:Profiler-interoperable web service for functional enrichment analysis and gene identifier mapping (2023 update). *Nucleic Acids Res*. 2023;51(W1):W207–12.
  58. Xiao Z, Dai Z, Locasale JW. Metabolic landscape of the tumor microenvironment at single cell resolution. *Nat Commun*. 2019;10(1):3763.
  59. Lun AT, Bach K, Marioni JC. Pooling across cells to normalize single-cell RNA sequencing data with many zero counts. *Genome Biol*. 2016;17:75.
  60. van Dijk D, Sharma R, Nainys J, Yin K, Kathail P, Carr AJ, et al. Recovering gene interactions from single-cell data using data diffusion. *Cell*. 2018;174(3):716–29.e27.
  61. Wagner A, Wang C, Fessler J, DeTomaso D, Avila-Pacheco J, Kaminski J, et al. Metabolic modeling of single Th17 cells reveals regulators of autoimmunity. *Cell*. 2021;184(16):4168–85.e21.
  62. Jin S, Guerrero-Juarez CF, Zhang L, Chang I, Ramos R, Kuan CH, et al. Inference and analysis of cell-cell communication using Cell Chat. *Nat Commun*. 2021;12(1):1088.
  63. Phillips RA, Tüscher JJ, Black SL, Andracka E, Fitzgerald ND, Janov L, et al. An atlas of transcriptionally defined cell populations in the rat ventral tegmental area. *Cell Rep*. 2022;39(1):110616.
  64. Bergen V, Lange M, Peidli S, Wolf FA, Theis FJ. Generalizing RNA velocity to transient cell states through dynamical modeling. *Nat Biotechnol*. 2020;38(12):1408–14.
  65. La Manno G, Soldatov R, Zeisel A, Braun E, Hochgerner H, Petukhov V, et al. RNA velocity of single cells. *Nature*. 2018;560(7719):494–8.
  66. Masuda T, Sankowski R, Staszewski O, Prinz M. Microglia heterogeneity in the single-cell era. *Cell Rep*. 2020;30(5):1271–81.
  67. Safaiyan S, Besson-Girard S, Kaya T, Cantuti-Castelvetri L, Liu L, Ji H, et al. White matter aging drives microglial diversity. *Neuron*. 2021;109(7):1100–17.e10.
  68. Ximerakis M, Lipnick SL, Innes BT, Simmons SK, Adiconis X, Dionne D, et al. Single-cell transcriptomic profiling of the aging mouse brain. *Nat Neurosci*. 2019;22(10):1696–708.
  69. Deczkowska A, Keren-Shaul H, Weiner A, Colonna M, Schwartz M, Amit I. Disease-associated microglia: a universal immune sensor of neurodegeneration. *Cell*. 2018;173(5):1073–81.
  70. Depp C, Sun T, Sasmita AO, Spieth L, Berghoff SA, Nazarenko T, et al. Myelin dysfunction drives amyloid-beta deposition in models of Alzheimer's disease. *Nature*. 2023;618(7964):349–57.
  71. Borst K, Schwabenland M, Prinz M. Microglia metabolism in health and disease. *Neurochem Int*. 2019;130:104331.
  72. Bradbury EJ, Moon LD, Popat RJ, King VR, Bennett GS, Patel PN, et al. Chondroitinase ABC promotes functional recovery after spinal cord injury. *Nature*. 2002;416(6881):636–40.
  73. Barritt AW, Davies M, Marchand F, Hartley R, Grist J, Yip P, et al. Chondroitinase ABC promotes sprouting of intact and injured spinal systems after spinal cord injury. *J Neurosci*. 2006;26(42):10856–67.
  74. Fouad K, Schnell L, Bunge MB, Schwab ME, Liebscher T, Pearse DD. Combining Schwann cell bridges and olfactory-ensheathing glia grafts with chondroitinase promotes locomotor recovery after complete transection of the spinal cord. *J Neurosci*. 2005;25(5):1169–78.
  75. Crapser JD, Ochaba J, Soni N, Reidling JC, Thompson LM, Green KN. Microglial depletion prevents extracellular matrix changes and



- striatal volume reduction in a model of Huntington's disease. *Brain*. 2020;143(1):266–88.
76. Tansley S, Gu N, Guzman AU, Cai W, Wong C, Lister KC, et al. Microglia-mediated degradation of perineuronal nets promotes pain. *Science*. 2022;377(6601):80–6.
  77. Crapser JD, Spangenberg EE, Barahona RA, Arreola MA, Hohsfield LA, Green KN. Microglia facilitate loss of perineuronal nets in the Alzheimer's disease brain. *EBioMedicine*. 2020;58: 102919.
  78. Bellver-Landete V, Bretheau F, Mailhot B, Vallieres N, Lessard M, Janelle ME, et al. Microglia are an essential component of the neuroprotective scar that forms after spinal cord injury. *Nat Commun*. 2019;10(1):518.
  79. Fan Y, Wu X, Han S, Zhang Q, Sun Z, Chen B, et al. Single-cell analysis reveals region-heterogeneous responses in rhesus monkey spinal cord with complete injury. *Nat Commun*. 2023;14(1):4796.
  80. Cserep C, Posfai B, Lenart N, Fekete R, Laszlo ZI, Lele Z, et al. Microglia monitor and protect neuronal function through specialized somatic purinergic junctions. *Science*. 2020;367(6477):528–37.
  81. Zhan Y, Paolicelli RL, Sforzini F, Weinhard L, Bolasco G, Pagani F, et al. Deficient neuron-microglia signaling results in impaired functional brain connectivity and social behavior. *Nat Neurosci*. 2014;17(3):400–6.
  82. Tremblay ME, Lowery RL, Majewska AK. Microglial interactions with synapses are modulated by visual experience. *PLoS Biol*. 2010;8(11): e1000527.
  83. Schafer DP, Lehrman EK, Kautzman AG, Koyama R, Mardinly AR, Yamasaki R, et al. Microglia sculpt postnatal neural circuits in an activity and complement-dependent manner. *Neuron*. 2012;74(4):691–705.
  84. Townley RA, Boeve BF, Benarroch EE. Progranulin: functions and neurologic correlations. *Neurology*. 2018;90(3):118–25.
  85. Van Damme P, Van Hoecke A, Lambrechts D, Vanacker P, Bogaert E, van Swieten J, et al. Progranulin functions as a neurotrophic factor to regulate neurite outgrowth and enhance neuronal survival. *J Cell Biol*. 2008;181(1):37–41.
  86. Naphade SB, Kigerl KA, Jakeman LB, Kostyk SK, Popovich PG, Kuret J. Progranulin expression is upregulated after spinal contusion in mice. *Acta Neuropathol*. 2010;119(1):123–33.
  87. Wang C, Zhang L, Ndong JC, Hettinghouse A, Sun G, Chen C, et al. Progranulin deficiency exacerbates spinal cord injury by promoting neuroinflammation and cell apoptosis in mice. *J Neuroinflammation*. 2019;16(1):238.
  88. Ozdinler PH, Macklis JD. IGF-I specifically enhances axon outgrowth of corticospinal motor neurons. *Nat Neurosci*. 2006;9(11):1371–81.
  89. Liu Y, Wang X, Li W, Zhang Q, Li Y, Zhang Z, et al. A Sensitized IGF1 treatment restores corticospinal axon-dependent functions. *Neuron*. 2017;95(4):817–33.e4.
  90. Brennan FH, Swarts EA, Kigerl KA, Mifflin KA, Guan Z, Noble BT, et al. Microglia promote maladaptive plasticity in autonomic circuitry after spinal cord injury in mice. *Sci Transl Med*. 2024;16(751):eadi3259.
  91. Krajacic A, Ghosh M, Puentes R, Pearce DD, Fouad K. Advantages of delaying the onset of rehabilitative reaching training in rats with incomplete spinal cord injury. *Eur J Neurosci*. 2009;29(3):641–51.
  92. Torres-Espin A, Forero J, Schmidt EKA, Fouad K, Fenrich KK. A motorized pellet dispenser to deliver high intensity training of the single pellet reaching and grasping task in rats. *Behav Brain Res*. 2018;336:67–76.
  93. Wang Y, Su H, Zhong J, Zhan Z, Zhao Q, Liu Y, et al. Osteopontin enhances the effect of treadmill training and promotes functional recovery after spinal cord injury. *Mol Biomed*. 2023;4(1):44.
  94. Byrnes KR, Washington PM, Knobloch SM, Hoffman E, Faden AI. Delayed inflammatory mRNA and protein expression after spinal cord injury. *J Neuroinflammation*. 2011;8:130.
  95. Andrews EM, Richards RJ, Yin FQ, Viapiano MS, Jakeman LB. Alterations in chondroitin sulfate proteoglycan expression occur both at and far from the site of spinal contusion injury. *Exp Neurol*. 2012;235(1):174–87.
  96. Jones LL, Tuszynski MH. Spinal cord injury elicits expression of keratan sulfate proteoglycans by macrophages, reactive microglia, and oligodendrocyte progenitors. *J Neurosci*. 2002;22(11):4611–24.
  97. Jones LL, Margolis RU, Tuszynski MH. The chondroitin sulfate proteoglycans neurocan, brevican, phosphacan, and versican are differentially regulated following spinal cord injury. *Exp Neurol*. 2003;182(2):399–411.
  98. McKeon RJ, Schreiber RC, Rudge JS, Silver J. Reduction of neurite outgrowth in a model of glial scarring following CNS injury is correlated with the expression of inhibitory molecules on reactive astrocytes. *J Neurosci*. 1991;11(11):3398–411.
  99. Crespo D, Asher RA, Lin R, Rhodes KE, Fawcett JW. How does chondroitinase promote functional recovery in the damaged CNS? *Exp Neurol*. 2007;206(2):159–71.
  100. Dyck SM, Karimi-Abdolrezaee S. Chondroitin sulfate proteoglycans: Key modulators in the developing and pathologic central nervous system. *Experiment Neurol*. 2015;269:169–87.
  101. Sanchez-Ventura J, Lane MA, Udina E. The role and modulation of spinal perineuronal nets in the healthy and injured spinal cord. *Front Cell Neurosci*. 2022;16: 893857.
  102. Schmidt E, Raposo P, Vavrek R, Fouad K. Inducing inflammation following subacute spinal cord injury in female rats: a double-edged sword to promote motor recovery. *Brain Behav Immun*. 2021;93:55–65.
  103. Kozłowski P, Rosicka P, Liu J, Yung AC, Tetzlaff W. In vivo longitudinal Myelin Water Imaging in rat spinal cord following dorsal column transection injury. *Magn Reson Imaging*. 2014;32(3):250–8.
  104. Becerra JL, Puckett WR, Hiester ED, Quencer RM, Marcillo AE, Post MJ, et al. MR-pathologic comparisons of wallerian degeneration in spinal cord injury. *AJNR Am J Neuroradiol*. 1995;16(1):125–33.
  105. Vallieres N, Berard JL, David S, Lacroix S. Systemic injections of lipopolysaccharide accelerates myelin phagocytosis during Wallerian degeneration in the injured mouse spinal cord. *Glia*. 2006;53(1):103–13.
  106. Schnell L, Schwab ME. Axonal regeneration in the rat spinal cord produced by an antibody against myelin-associated neurite growth inhibitors. *Nature*. 1990;343(6255):269–72.
  107. Schwab ME. Nogo and axon regeneration. *Curr Opin Neurobiol*. 2004;14(1):118–24.
  108. Sicotte M, Tsatas O, Jeong SY, Cai CQ, He Z, David S. Immunization with myelin or recombinant Nogo-66/MAG in alum promotes axon regeneration and sprouting after corticospinal tract lesions in the spinal cord. *Mol Cell Neurosci*. 2003;23(2):251–63.
  109. Vargas ME, Barres BA. Why is Wallerian degeneration in the CNS so slow? *Annu Rev Neurosci*. 2007;30:153–79.
  110. Vargas ME, Watanabe J, Singh SJ, Robinson WH, Barres BA. Endogenous antibodies promote rapid myelin clearance and effective axon regeneration after nerve injury. *Proc Natl Acad Sci U S A*. 2010;107(26):11993–8.
  111. Plemel JR, Keough MB, Duncan GJ, Sparling JS, Yong VW, Stys PK, et al. Remyelination after spinal cord injury: is it a target for repair? *Prog Neurobiol*. 2014;117:54–72.
  112. Kotter MR, Li WW, Zhao C, Franklin RJ. Myelin impairs CNS remyelination by inhibiting oligodendrocyte precursor cell differentiation. *J Neurosci*. 2006;26(1):328–32.
  113. Kotter MR, Setzu A, Sim FJ, Van Rooijen N, Franklin RJ. Macrophage depletion impairs oligodendrocyte remyelination following lysolecithin-induced demyelination. *Glia*. 2001;35(3):204–12.
  114. Duncan GJ, Manesh SB, Hilton BJ, Assinck P, Liu J, Moulson A, et al. Locomotor recovery following contusive spinal cord injury does not require oligodendrocyte remyelination. *Nat Commun*. 2018;9(1):3066.
  115. Assinck P, Duncan GJ, Hilton BJ, Plemel JR, Tetzlaff W. Cell transplantation therapy for spinal cord injury. *Nat Neurosci*. 2017;20(5):637–47.
  116. Tetzlaff W, Okon EB, Karimi-Abdolrezaee S, Hill CE, Sparling JS, Plemel JR, et al. A systematic review of cellular transplantation therapies for spinal cord injury. *J Neurotrauma*. 2011;28(8):1611–82.
  117. Wu YQ, Xiong J, He ZL, Yuan Y, Wang BN, Xu JY, et al. Metformin promotes microglial cells to facilitate myelin debris clearance and accelerate nerve repairment after spinal cord injury. *Acta Pharmacol Sin*. 2022;43(6):1360–71.

## Publisher's Note

Springer Nature remains neutral with regard to jurisdictional claims in published maps and institutional affiliations.